PERGAMON

Vacuum 64 (2002) 119–144

VACUUM
SURFACE ENGINEERING, SURFACE INSTRUMENTATION & VACUUM TECHNOLOGY

www.elsevier.com/locate/vacuum

Wake vacuum measurement and analysis for the wake shield facility free flying platform

J.A. Strozier[1], M. Sterling, J.A. Schultz[2], A. Ignatiev*

Space Vacuum Epitaxy Center, Texas Center for Superconductivity, University of Houston, Houston, TX 77204-5507, USA

Abstract

We report here the temperature and pressure measurements recorded on the Wake Shield Facility (WSF) during the two flights in which it was a free flyer in low earth orbit. The WSF is a disk-shaped platform on which are attached, on the wake side, apparatus necessary for the epitaxial growth of thin film materials. Previous calculations suggest that the pressure on the wake side could be decreased by some 6 orders of magnitude over the ambient pressure in low earth orbit (from 10^{-8} to 10^{-14} Torr). Analysis of the pressure and temperature data gathered from the two flights and presented here concludes that the decrease was some 2 orders of magnitude or 4 orders of magnitude less than expected. Reasons for this discrepancy are proposed and it is suggested that the original pressure values could be reached if, prior to growth, the WSF was sufficiently outgassed.

1. Introduction

1.1. Original concept

Vacuum, one of the major attributes of space, has heretofore been principally perceived as detrimental to space operations. However, in the early 1970s scientists focused on the possibility of generating near-perfect vacuum in low earth orbit space in the wake of an orbiting vehicle [1–4]. This concept of space ultra-vacuum was further amplified by Ignatiev et al. [5–8], in a program to utilize space ultra-vacuum for the fabrication of high purity epitaxial thin film materials grown on board a specifically developed disc-shaped platform, the Wake Shield Facility (WSF) by molecular beam epitaxy (MBE) [9]. The wake vacuum data collected on the flights of the WSF is presented here, and compared to both past predictions and current analysis.

In 1976, Melfi et al. [2] and Hueser and Brock [3] proposed that a semi-hemispherical shell in low earth orbit, oriented so that the convex (closed) part of the shell faced the direction of motion, would create a vacuum in the interior of the shell which would approach a limiting pressure of some 10^{-14} Torr. They analyzed the pressure at the center of the shell due to the free stream atmosphere using the kinetic theory of a drifting Maxwellian gas. Since the orbiting shell moves at a speed of approximately 10 times the speed of the ambient gas molecules (mostly atomic oxygen), a greatly reduced ambient gas density will be left in the wake region.

*Corresponding author. Tel.: +1-713-743-3621; fax: +1-713-747-7724.

E-mail address: ignatiev@uh.edu (A. Ignatiev).

[1] Permanent address: SUNY Empire State College, Hauppauge, NY 11788-5539, USA.

[2] With: Ionwerks, Inc., 2472 Bolsover, Suite255, Houston, TX 77005, USA.

0042-207X/01/$-see front matter
PII: S0042-207X(01)00383-9

They also considered the contribution to the pressure from three other gas sources: outgassing from the inner surface of the shield; gas released by an experiment; and atmospheric gas scattered off the orbiter.

Somewhat later, in a series of papers, Naumann [4] proposed a slightly different design for a dish behind which MBE could be undertaken in which the concave (open) side of the orbiting shell was orientated towards the direction of flight (the ram side). This orientation eliminated from the sample the direct flux of species desorbed from the shield itself. However flux from direct line-of-sight packages MBE growth assembly and/or surface diagnostic instruments assembly, when in their active positions, was not taken into account. In Naumann's proposal, the shell would be inserted into low earth orbit by the Space Shuttle Orbiter.

The conclusions of Melfi et al., Hueser and Brock, and Naumann were that pressures of the order of 10^{-14} Torr were indeed possible in the wake of the disc. For this to happen, Melfi et al. and Hueser and Brock required that the outgassing rate of the interior of the shell be kept to values below 3×10^7 particles/cm^2 s, a rate that is at the very low end of measured outgassing rates for "thoroughly degassed stainless steel" [3]. On the other hand, Naumann required only that the shell be a free flyer; positioned some distance from the Orbiter; which, he projected, is a significant source of contaminating species (mostly water).

1.2. Monte Carlo calculations

In a series of papers from 1991 to 1993 Justiz et al. [10,11] using a "Direct Simulation Monte Carlo Technique" calculated the various species concentrations about a 12 ft flat disk in low earth orbit oriented perpendicular to the direction of flight. Note that the geometry is somewhat different from that proposed by either Melfi et al. or Naumann. In particular, the flat geometry is both an aid to calculation and, as with the Naumann model, does not present any viewing surface to the wake side. Thus particles outgassing from the wake side surface would simply move away from the surface and not become incident on any part of the wake side surface where experiments utilizing the wake vacuum could be done. In the Justiz et al. model, all particles incident on the wake side must come only from the free stream atmosphere (both directly and those backscattered from particles desorbing from the shield itself), and from outgassing of the Orbiter (if near enough). Not considered in this calculation was outgassing from surfaces which could be seen by the wake surface and these would include any experimental apparatus built up on the wake side such as the MBE growth assembly and surface diagnostic instruments.

The results of the Monte Carlo simulations were that a 12 ft disk in low earth orbit oriented perpendicular to the direction of flight would produce an order of magnitude increase in the pressure on the ram side, and a six orders of magnitude decrease in the pressure on the wake side at the surface of the disk. This would yield pressures on the wake side of the order of 10^{-14} Torr, and on the ram side of 10^{-7} Torr in agreement with the previous results of Melfi, Hueser, Brock, and Naumann.

1.3. The actual experiment

The wake ultra-vacuum concept, as proposed and theoretically analyzed by the several groups above, was actually put to an experimental test in a series of three low earth orbit flights of the WSF. These flights occurred on Space Shuttle Flight STS 60 (Discovery, February 3–11, 1994), Flight STS 69 (Endeavour, September 7–18, 1995), and Flight STS 80 (Columbia, November 19–December 5, 1996).

The WSF is an orientable stainless steel platform (geometry similar to that used by Justiz et al.) on which are attached various measuring instruments (temperature, pressure, magnetic field, acceleration) and the experimental apparatus necessary for molecular beam epitaxial growth of thin film materials on the wake side and atomic oxygen reactions on the ram side.

The WSF was carried into low earth orbit by the Orbiter to approximately 200 miles altitude where the average pressure, due mostly to atomic oxygen, is about 1×10^{-8} Torr. In the first flight, the WSF remained on the Orbiter arm with its ram side

facing the direction of motion. In the second and third flights, the WSF became a free flyer. After release by the Orbiter, the WSF moved some distance (20–40 miles) behind the Orbiter to minimize both ambient gas scattered from the Orbiter as well as outgassing from the Orbiter itself. When the experiments on board WSF were completed, it was picked up by the Orbiter, berthed in the payload bay, and returned to earth.

We first give a brief summary of the results: (1) Analysis of the rather large amount of temperature and pressure data gathered on the three flights strongly supports the wake vacuum formation concept: i.e. that the pressure on the wake side is greatly reduced over that on the ram side and that of the ambient free stream atmosphere. (2) The average value of the ram pressure is increased by an order of magnitude as predicted by the Monte Carlo simulations, and the wake side pressure is decreased by two orders of magnitude, which is significantly less than the 6 orders of magnitude predicted by calculations.

In order to both support these conclusions and propose an explanation for the discrepancy in the expected decrease in pressure on the wake side, we will detail the pressure and temperature data, and present a theoretical analysis of the pressure distribution on the WSF. The analysis is based on a model of thermal solar outgassing of particles from the wake side of the shield and subsequent reflection of a fraction of those particles from the molecular beam growth assembly during the flights. We also considered internal outgassing in the gauges themselves. The results of the analysis of the data and the correlation with the proposed model provide a reasonable explanation for the measured average (dc) levels of pressure and their variations with time.

2. Wake Shield Facility hardware

The WSF is a 12 ft 304L stainless steel disk-shaped platform for growing crystalline thin film materials by MBE. It flies in a low earth orbit in free flight with the plane of the disk perpendicular to the direction of flight, creating a wake vacuum on the wake side and a buildup of pressure on the ram side (see Fig. 1). At the orbital altitude of 215 nautical miles, the atmospheric diurnal variation of the pressure due to the heating of the atmosphere by the sun is the order of its average value which is approximately 10^{-8} Torr [12,13].

The WSF is equipped with four total pressure gauges which consist of two Kernco [14] cold-cathode pressure gauges with limiting pressure reading of about 1×10^{-8} Torr and two Balzers [15] cold-cathode pressure gauges with a limiting pressure reading of about 1×10^{-9} Torr [16]. These are located on the WSF as follows (see Fig. 2): Kernco gauge #1 (K1) is located on the ram side near the Z axis at the edge of the WSF. The wake side supports Kernco #2 (K2), located close to the sample near the center of the WSF and the two Balzers gauges which are located along the Z axis. Balzers guage #2 (B2) is near the outer edge of the WSF, and Balzers gauge #1 (B1) is located towards the center at the edge of the growth assembly (about half-way to the center of the WSF).

All of the total pressure gauges were sampled every 5 s during WSF flight operations with the results returned to earth for storage via a communications link. Since an orbital period was about 1.54 h, over 1000 pressure data points were recorded per pressure gauge per orbital period yielding a reasonably continuous description of the pressure on the WSF as a function of time.

The sample holder, called the *carousel*, and the molecular beam *source cell assembly* are shown in Fig. 3. Seven GaAs substrates, on which epitaxial films were grown, were mounted in the carousel assembly. Each substrate, with its individual heater, could be rotated and locked into the

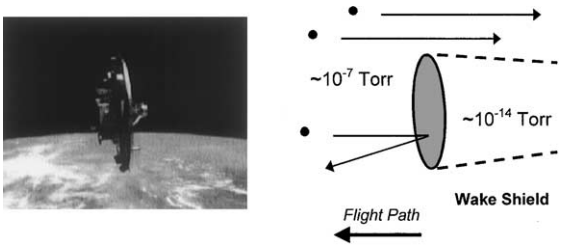

Fig. 1. On the left side of the figure is a photograph of the WSF in flight. An idealized schematic of the WSF space wake formation is on the right.

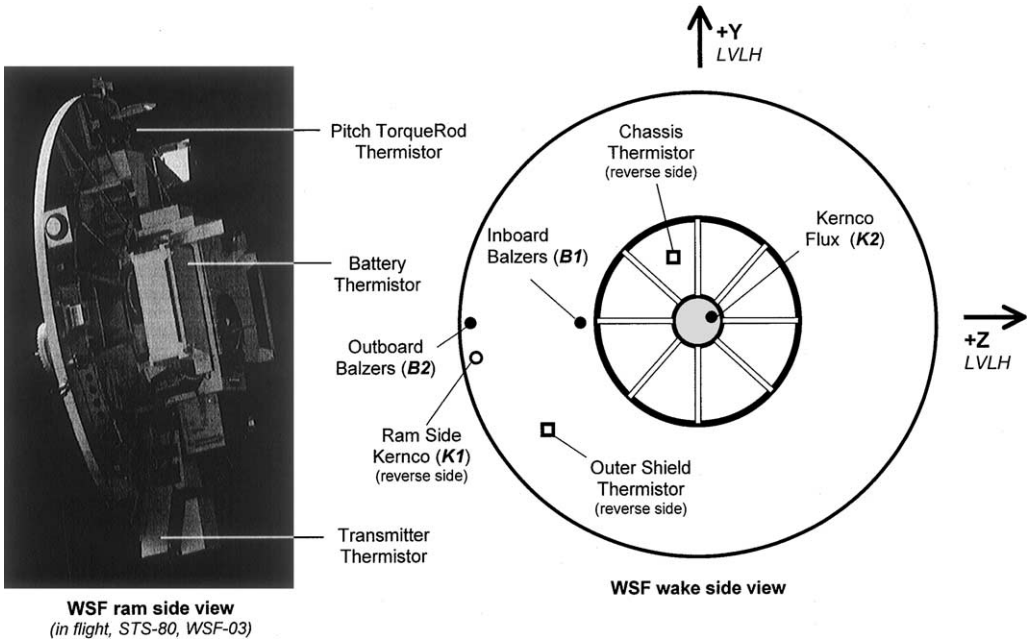

Fig. 2. Top view of the wake side of WSF with inset of a photograph of the ram side of the actual WSF. Shown are the location of the Kernco flux (K2), the inboard Balzers (B1), and the outboard Balzers (B2) total pressure gauges as well as the location of the ram side Kernco (K1) gauge. Also located are the chassis and outer shield thermistors. The pitch torquerod, battery, and transmitter thermistors on the ram side are located on the photograph. In flight, the Z coordinate is the vector from the center of the earth through the middle of the WSF, the X coordinate (not shown) is the vector in the flight direction passing through the center of the WSF and perpendicular to its plane, and the Y coordinate is perpendicular to both X and Z.

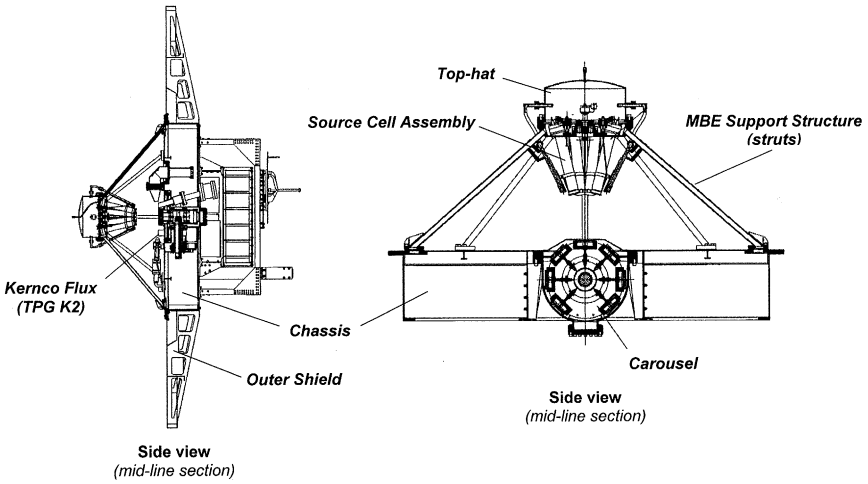

Fig. 3. Side view of the WSF showing the source cell or growth assembly, the Top-hat, the MBE support structure called the struts, the carousel, chassis, and outer shield.

growth position. The carousel is located at the origin (center) of the WSF. When a substrate is locked into the growth position, it is at the level of the wake side of the WSF and looks directly at the source cell assembly and into space. The source cell assembly consists of a cluster of eight molecular beam source cells on top of which is the *Top-hat* assembly. The source cell assembly is mounted on eight rods, called the *struts*, so that the center line of the source cell assembly passed through the center of the sample locked in the growth position.

The section of the WSF between the carousel and the struts is called the *chassis*, and that between the chassis and the outer edge of the WSF the *outer shield*.

3. Pressure and temperature data

We first plot the pressure and temperature values measured on board the WSF as a function of time for the duration of flights WSF-02 and WSF-03. The *ram* side pressure and temperature data from the total pressure gauge K1 and from several ram side thermistors are plotted in Fig. 4a and b (WSF-02) and Fig. 5a and b (WSF-03). The *wake* side pressure and temperature data from the total pressure gauges K2, B1, and B2 and from thermistors positioned on the outer shield, chassis, and Top-hat, are given in Fig. 6a and b (WSF-02) and Fig. 7a and b (WSF-03).

The most striking feature in Figs. 4–7 is the large diurnal variation (variation with period equal to a solar day as viewed from the WSF in orbital flight) in *all* the data, pressure and temperature values alike. We also note that the diurnal variation in the data from the *wake* side is phase shifted with respect to the data from the *ram* side by about 1/4 of an orbital period.

In addition to the diurnal variation, we note a one to two orders of magnitude increase in the wake side pressure which is coincident with the heating of the source cell assembly and the chassis/carousel (sample holder) during the degass and the growth phase of the MBE operations.

Very roughly we note that the *wake* side pressure curves of Figs. 6a and 7a follow the *wake* side temperature curves of Figs. 6b and 7b. Somewhat more specifically, one can say that the diurnal variation in the pressure follows most closely the outer shield temperature and the long term variation (dc) follows most closely the chassis temperature.

In the following three sections we will look at the correlations between the pressure and temperature data and the sun position relative to the WSF. These correlations lend support to the solar thermal desorption model which we propose to explain the pressure data.

3.1. Diurnal temperature data

As we have pointed out, measurements of the temperature versus time at several locations on the WSF during the flight show a pronounced diurnal variation. At the low variation end, the avionics pallet shows a diurnal variation of approximately 5°C (Fig. 8). At the high variation end, the diurnal variation measured on the outer shield skin of the WSF-02 is about 70°C (Fig. 6b). A simple thermal model of the WSF as an orbiting circular 304L stainless steel disk of thickness 0.059 in yields a diurnal variation of about 100°C with phase and shape very similar to the measured values in Fig. 6b. In this model the temperature difference between the ram and wake surfaces was calculated to be less than 0.02°C and is thereby neglected. The center portion of the WSF contains the electronics, batteries, structural components, etc. so that the ratio of its thermal mass to exposed area is such that the above approximation does not hold; hence, the difference between the diurnal temperature variation in Figs. 6b and 8.

We also note from the data that there is always a *maximum* in temperature at any point on the *wake* side of the WSF at orbital *sunset*, and a *minimum* in temperature at any point on the *ram* side of the WSF at orbital *sunrise*. In addition, we also note a dip in the temperature of the outer shield around orbital noon. These observations are in agreement with general thermal analysis considerations. At orbital sunset, the WSF is cutoff from solar heating until orbital sunrise at which time solar heating begins on the ram side and passes to the wake side at orbital noon. Around orbital noon

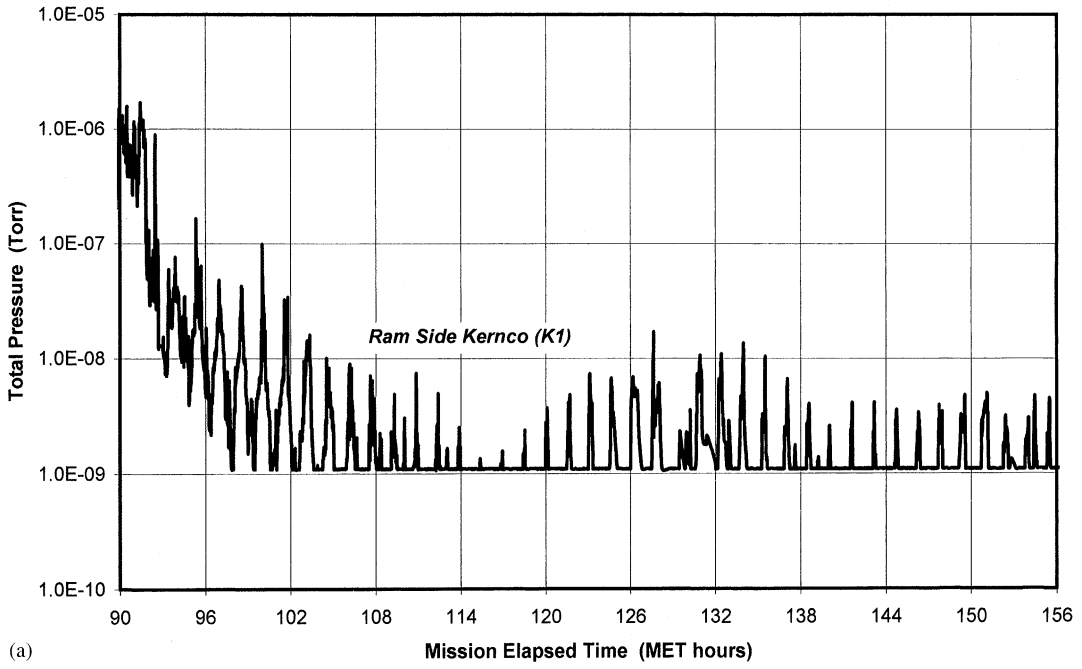

(a)

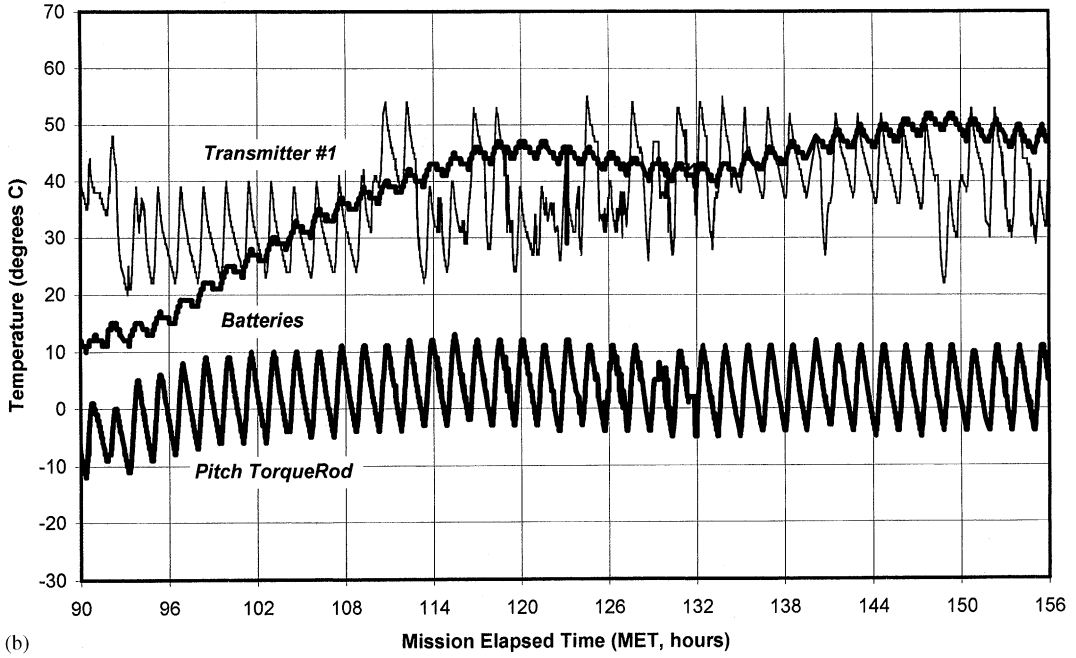

(b)

Fig. 4. (a) Ram side pressure data from Kernco total pressure gauge K1 plotted as a function of MET for the entire WSF-02 flight. Note the large diurnal variation per orbital period of 1.54 h. The gauge bottoms out at about 1E−09 Torr. (b) Ram side temperature data from thermistors located on transmitter #1, the battery pack, and the pitch torque rod plotted as a function of MET for the entire WSF-02 flight. Note also the large diurnal variation per orbital period as in (a). The erratic behavior of transmitter #1 during portions of the flight is due to communication problems.

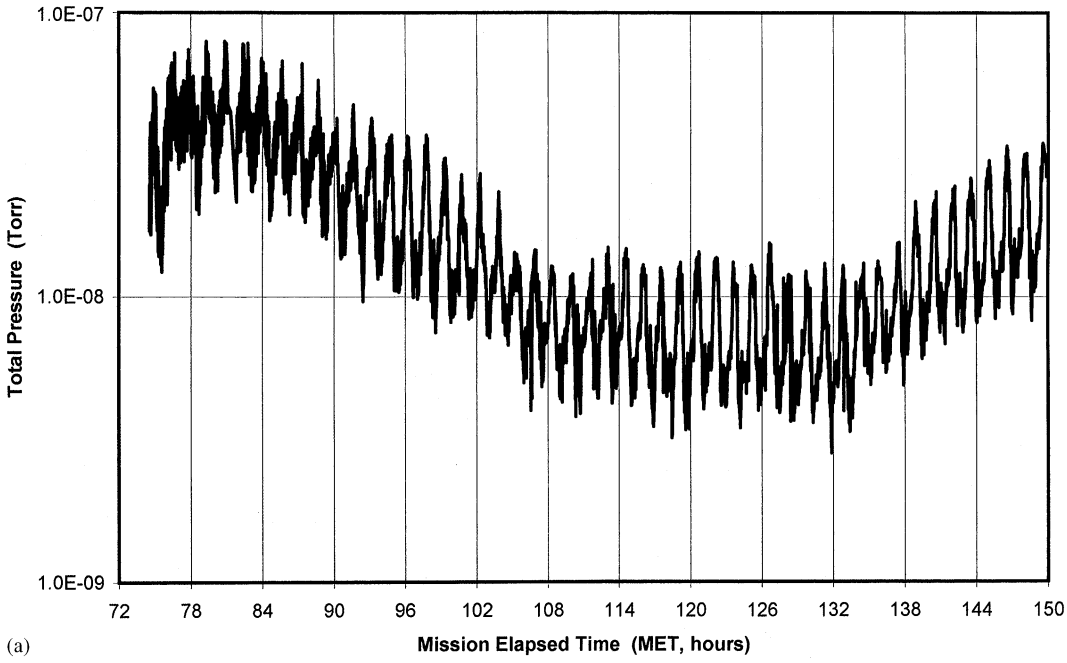

(a)

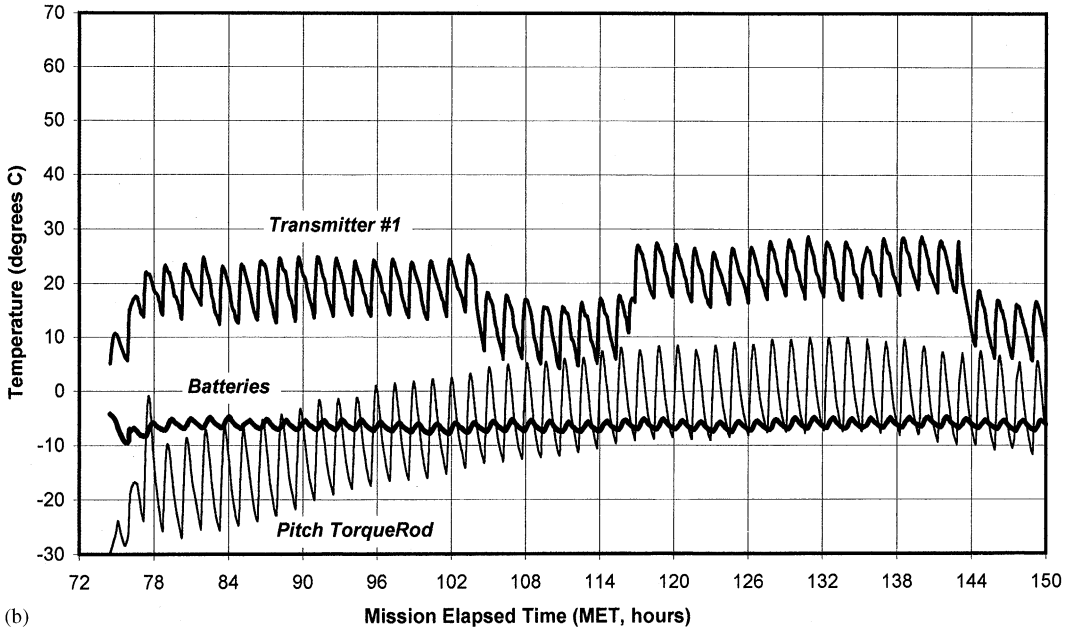

(b)

Fig. 5. (a) Ram side pressure data from Kernco total pressure gauge K1 plotted as a function of MET for the entire WSF-03 flight. Note the large diurnal variation per orbital period of 1.54 h. (b) Ram side temperature data from thermistors located on transmitter #1, the battery pack, and the pitch torque rod plotted as a function of MET for the entire WSF-03 flight. Note also the large diurnal variation per orbital period as in (a). The reason for the two drops in temperature occurring between 104–160 and 144–150 MET is not known.

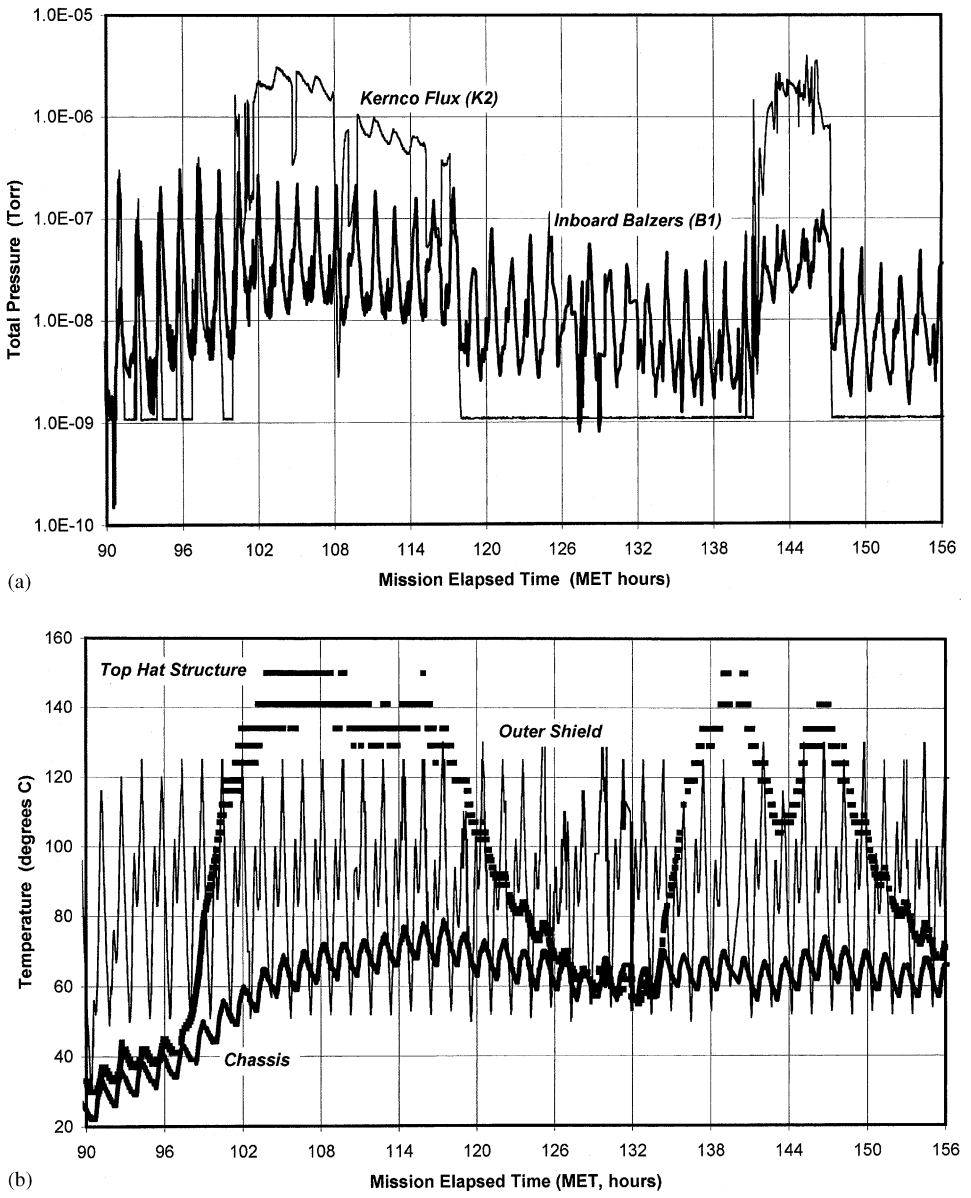

Fig. 6. (a) Wake side pressure data from the Kernco total pressure gauge K2 and the inboard Balzers gauge B1 plotted as a function of MET for the entire WSF-02 flight. Gauge K2, the flux gauge, is positioned close to the sample (near the center of the WSF) to measure the MBE flux to the sample, whereas Balzers gauge B1 is positioned halfway between the center of the WSF and its edge. Note the large diurnal variations per orbital period that are phase shifted by about 1/4 an orbital period with respect to the ram side data. Also note that during periods of growth, the pressure is substantially increased at the flux gauge K2. A substantially smaller increased pressure at B1 during growth is recorded as increased minimum values in the diurnal cycle. The reason for the erratic behavior in the flux gauge, K2, for the second growth phase is due to the fact that we had to go to manual control of the source cells. (b) Wake side temperature data from thermistors positioned on the outer shield, chassis, and Top-hat structure plotted as a function of time (MET) for the entire WSF-02 flight. A very strong diurnal variation is evident in the outer shield temperature data due to its low thermal mass per exposed area. In particular the 'blip' around orbital noon is clearly visible. Also the large increases and decreases of the temperature of the Top-hat structure correlate well with the growth periods during the flight.

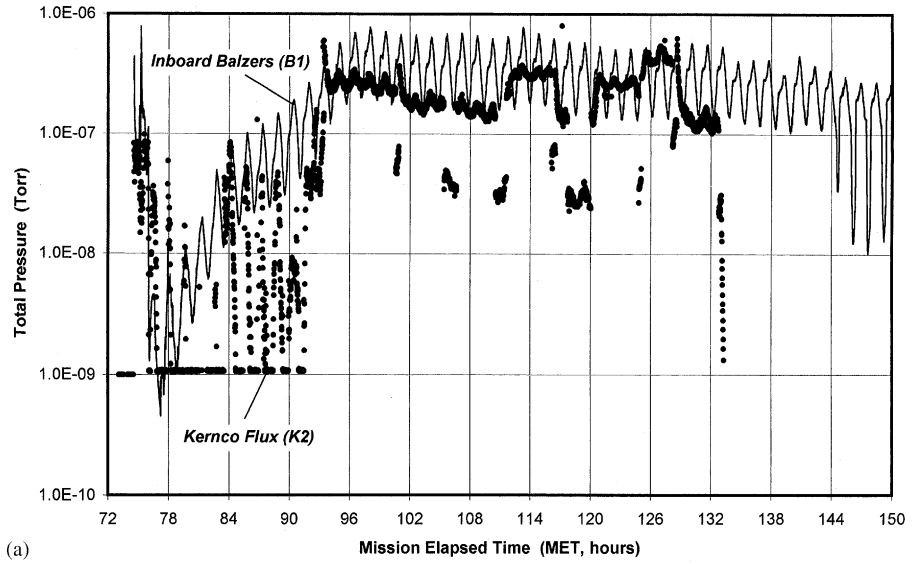

(a)

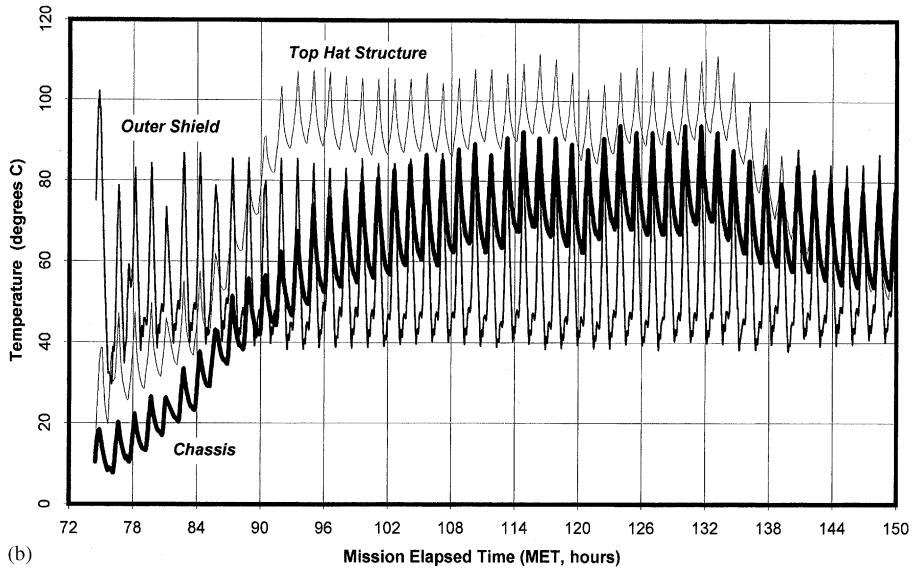

(b)

Fig. 7. (a) Wake side pressure data from the Kernco total pressure gauge K2 and the inboard Balzers gauge B1 plotted as a function of MET for the entire WSF-03 flight. Gauge K2 is positioned close to the sample near the center of the WSF, whereas Balzers gauge B1 is positioned half-way between the center of the WSF and its edge. Note the large diurnal variations per orbital period that are phase shifted by about 1/4 an orbital period with respect to the ram side data. Also note that during periods of growth, the pressure is substantially increased at K2 positioned to measure the flux close to the sample. Contrary to the data in WSF-02, both the DC and diurnal variation of the pressure as measured by B1 increases by over an order of magnitude beginning with the start of the growth phase and continuing until the end of the flight. (b) Wake side temperature data from thermistors positioned on the outer shield, chassis, and Top-hat structure plotted as a function of time (MET) for the entire WSF-03 flight. A very strong diurnal variation is evident in the outer shield temperature data due to its low thermal mass per exposed area. In particular the 'blip' around orbital noon is clearly visible although the rise in temperature before noon is not as great as in WSF-02. Also the large increase and decrease of the temperature of the Top-hat structure correlates with the growth period during the flight. Of particular interest is the increase in the diurnal variation in the chassis temperature which we attribute to a gallium coating beginning at the start of the growth phase (see text).

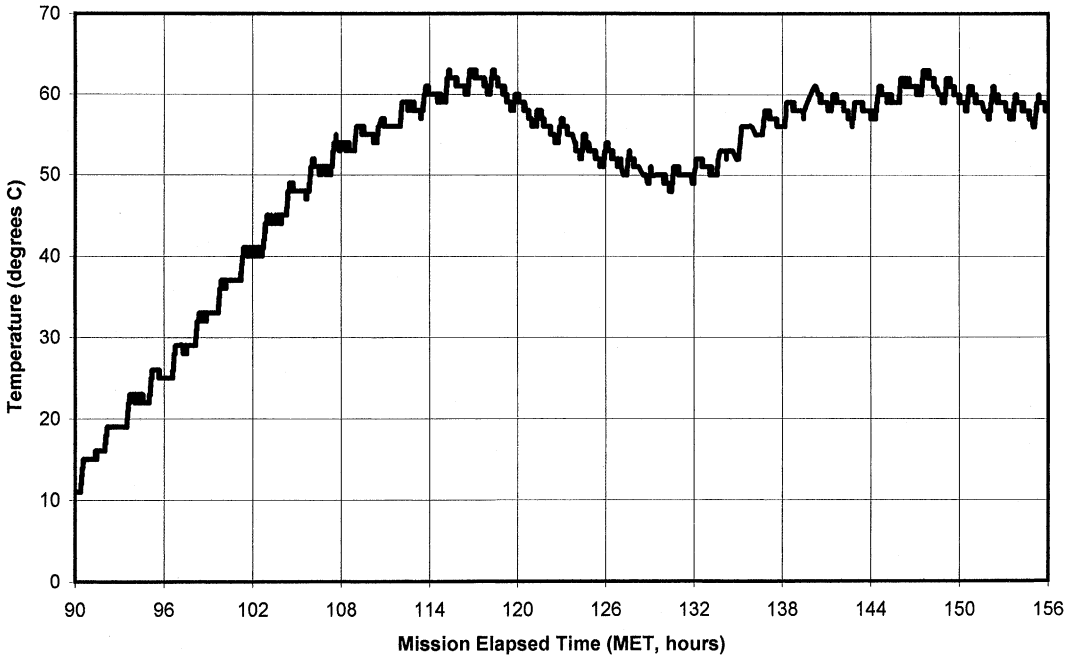

Fig. 8. Avionics Pallet temperature data for the entire WSF-02 flight. The pallet is in the interior section of the WSF facing the ram side. Note the small diurnal variation (about 5°C) due to its large thermal mass and small exposed area, and a much slower variation which correlates with the power drawn by the unit.

the sun is on the edge of the WSF. Thus solar heating incident on the WSF is at a maximum just before orbital sunset and just after sunrise, at a local minimum at around orbital noon, and zero between sunset and sunrise. The thin shield, receiving direct solar heating from the wake as well as the ram side, records a dip in temperature at the time of local minimum solar heating (around noon).

There is one anomaly in the temperature data that is important to mention. Note in Fig. 7b that the diurnal variation for the chassis in WSF-03 increases with time by a factor of 2, starting with the initiation of MBE operations at 90 mission elapsed time (MET) and reaching its steady state value at about 100 MET. This increase in the diurnal variation is not present in either the outer shield or the Top-hat, nor can it be connected to any increase in solar insolation. However, it is well to note that on WSF-03 the Ga source cell was excessively outgassed starting at about 90 h MET and, in fact, resulted in depletion of the Ga source cell. This resulted in a Ga coating on a major portion of the chassis. Visual inspection of the WSF after the WSF-03 flight suggests that the reflection coefficient for the Ga-covered stainless steel was noticeably less than that of the preflight electropolished original. Thus a larger portion of the solar insolation was absorbed by the chassis, resulting in a larger diurnal temperature variation observed on WSF-03.[3]

In summarizing this section we conclude from the data that the wake shield experiences diurnal temperature variations which can range from about 5°C to 70°C depending on the position on the WSF where the temperature is measured. These variations are in the proper phase with respect to the position of the sun to suggest that they are due to solar heating.

[3] In order for gallium coating of the stainless steel chassis to increase the diurnal variation by 10°C, the ratio of the absorption coefficient to the emissivity would have to increase by 13% above the value for polished stainless steel. In the light of visual inspection of the WSF after the flight, this is not unreasonable.

3.2. Ram side pressure data

The pressure on the ram side as measured by K1 versus time for the duration that WSF-02 was a free flyer is plotted in Fig. 4a. Note that the diurnal variation is of the order of the average value, which is roughly 10 times the expected ambient atomic oxygen pressure. Also the maximum in the diurnal variation is phase shifted to 2:00 p.m. local sun time and the minimum occurs at about 3:00 a.m. local sun time (see Fig. 9). The pressure amplitude, diurnal variation, and phase shifts are all consistent with the Jacchia 1970 model [12,13] (Fig. 9) for atmospheric solar heating.

The data of Fig. 4a also reveal an additional time dependence of the ram pressure (as measured by K1) which has a much longer period of variation and amplitude than the diurnal variation. In particular, the pressure first decreases with time from 90 MET hours (the beginning of the WSF activities) to about 118 MET hours. The pressure then increases until about 132 MET hours, after which it decreases to a steady state value. This long-term time dependence is explained by comparing this figure with Fig. 8, a plot of the temperature of the WSF avionics pallet as a function of time. The average pressure in Fig 4a follows very closely the inverse of the avionics pallet temperature. In fact we found (by independent calibration after the flight [17]) that the electronic gain of K2 is highly dependent on the temperature of the electronics hardware. As the temperature goes up the gain goes down by approximately a factor of 10 in pressure reading per 25°C increase in temperature. If this correction is taken into account, the actual ram pressure reading by K1 is essentially the diurnal variation imposed on a constant average pressure of approximately 10^{-7} Torr, as would be expected from the Jacchia model and a factor of 10 increase in pressure predicted by Justiz et al. on the ram side [10].

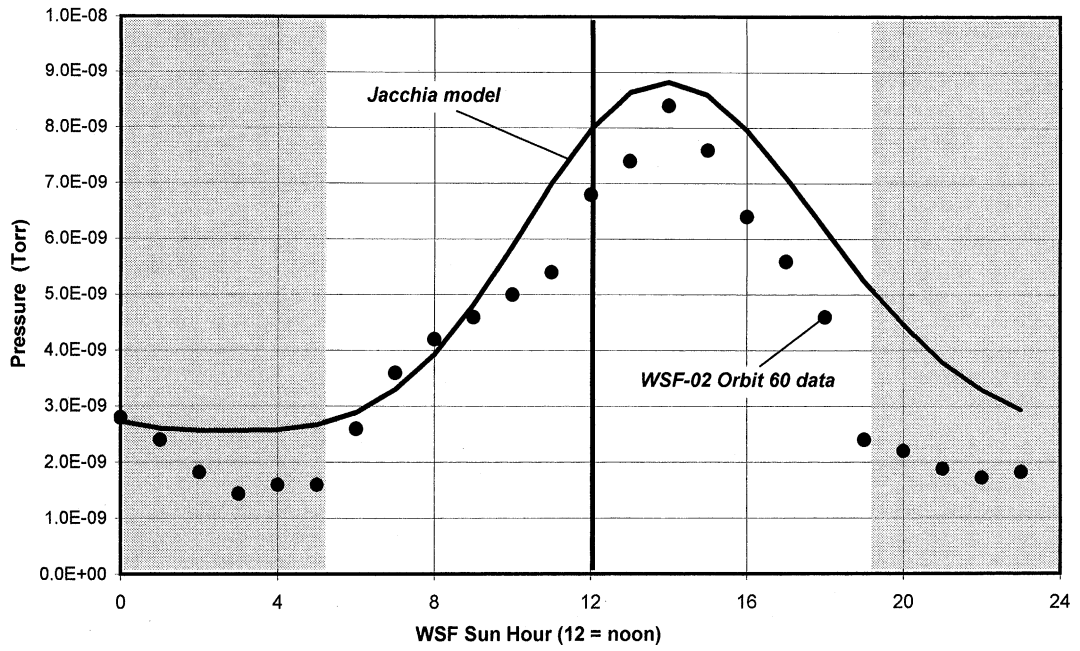

Fig. 9. Comparison of the ram pressure data from the Kernco guage K1, averaged over one orbital period with the Jacchia model of the atmospheric pressure at orbital altitude due to solar heating. While there are some variations in the K1 data, probably due to day/night heating, the maximum and minimum of both curves coincide and are located respectively at about 2:00 p.m. and 3:00 a.m. local (orbital) sun time.

3.3. Wake side pressure data

The time dependence of the wake side pressure and temperature data for WSF-02 are presented in expanded form in Fig. 10a and b including notation of orbital sunrise, sunset, and orbital noon. Included in these plots are the pressures measured by gauges K2, B1, and B2, and the temperatures of the shield, chassis, and Top-hat. Wake pressure and temperature data for WSF-03 are presented in Fig. 11a and b.

As previously noted, the most obvious feature is the large diurnal pressure variation which is phase shifted 23.7 min (lags in time and equal to about 1/4 of an orbit) with respect to the diurnal pressure variation on the ram side. Within the resolution of the data, this phase shift is the same for each of the three gauges on the wake side and is constant throughout both free flights (from 90 to 167 h MET for WSF-02 and from 74 to 150 h MET for WSF-03). In fact, we note that *all* temperature and pressure measurements on the wake side show *both* the temperature and pressure peaking at or very close to the sunset terminator (local sunset). This is quite different from the situation on the ram side where the ram pressure peaked at 2:00 p.m. local sun time (hence the diurnal pressure phase shift), and the temperature peaked at about local noon.

Not only is the phase of the pressure verses temperature suggestive of solar thermal outgassing, but so is the shape of the pressure peak after orbital sunset. Note that the decrease after sunset (Figs. 10a and 11a) is not abrupt but decreases monotonically until a short time after orbital sunrise. Furthermore, the pressure does not begin to increase rapidly until after orbital noon. Between the sunrise terminator and orbital noon, the sun is incident on the ram side of the WSF. Heat must then be conducted through the WSF to the wake side in order to raise its temperature. This can happen rapidly on the outer shield that is only 0.059 in thick. However, the interior section of the shield (the avionics palate) is populated with batteries, electronics, and other sub-assemblies, and about a third of the outer shield contains equipment and other payloads. In these areas, heat must pass through considerable thermal mass. After orbital noon, the sun is incident directly on the wake side of the shield and MBE growth assembly, and can heat them without any intermediate thermal mass. The solar heating continues with increasing heat input (the angle between the sun and the normal to the WSF decreases with time) until orbital sunset. The peak in pressure at orbital sunset coinciding with the peak in temperature of the various components on the wake side of the WSF strongly suggests that the diurnal pressure variation measured on the WSF is due to thermal outgassing of the WSF and its components by the sun.

Other details of the pressure plots reveal some differences between flights WSF-02 and WSF-03, so we will discuss each separately.

3.3.1. WSF-02

During the early part of the WSF-02 free flight before any thin film growth took place (Fig. 6a—90–95 h MET), the DC base pressure values on the wake side were 1×10^{-9} Torr for K2 (actually this gauge 'bottomed out' at this pressure), 2×10^{-9} Torr for the inboard Balzers, B1, and 4×10^{-10} Torr for the outboard Balzers, B2. Diurnal variations of the order of 100 times the base value of the pressure were also noted. During the warm-up, degas, and growth phases of the thin film growth on the wake side, as the source cells and substrates came up to temperature, the DC base pressures as measured by both Balzers gauges increased about an order of magnitude to 2×10^{-8} Torr for B1 and to 6×10^{-9} Torr for B2.

However, the Kernco K2 gauge (located on the Chassis to measure the flux from the source cells) pressure reading actually decreased from 90 to 100 h MET (Fig. 4a), tracking inversely the increase in temperature of the WSF, and specifically the temperature of the gauge electronics (see Fig. 8 and noted in the previous section). During thin film growth (Fig. 6a—from 100 to 118 h) the pressure increase from the source cells was sufficient to over-ride the heating of the electronics and a rise to 2×10^{-6} Torr was recorded at the beginning of the growth phase. The K2 gauge pressure then proceeded to decrease, again following the increase in temperature, until the end of the growth phase. At that point K2 became too hot for the incoming flux and the readings simply

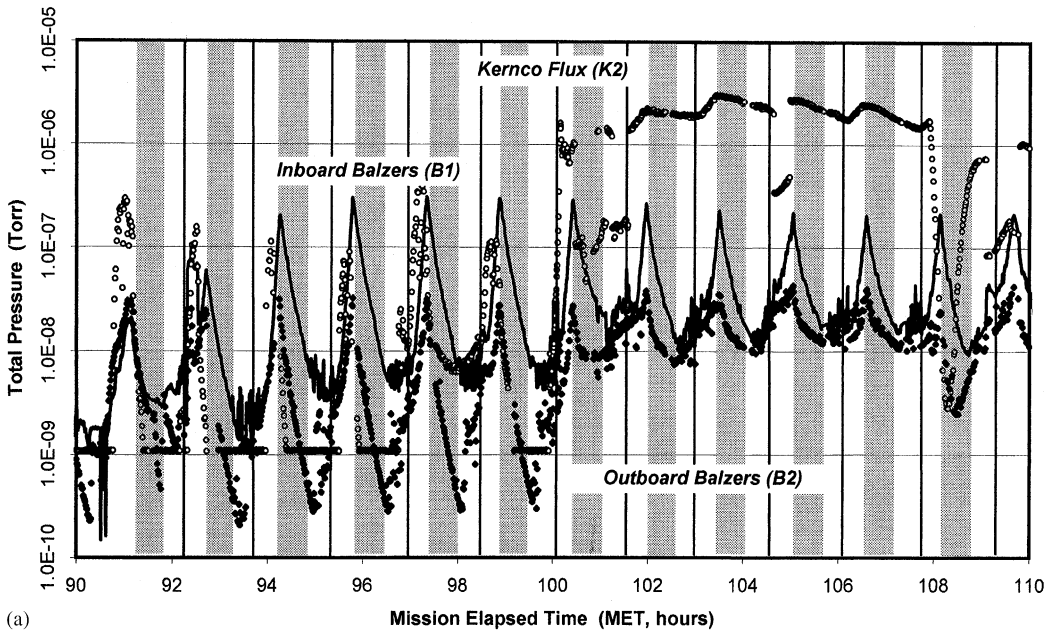

(a)

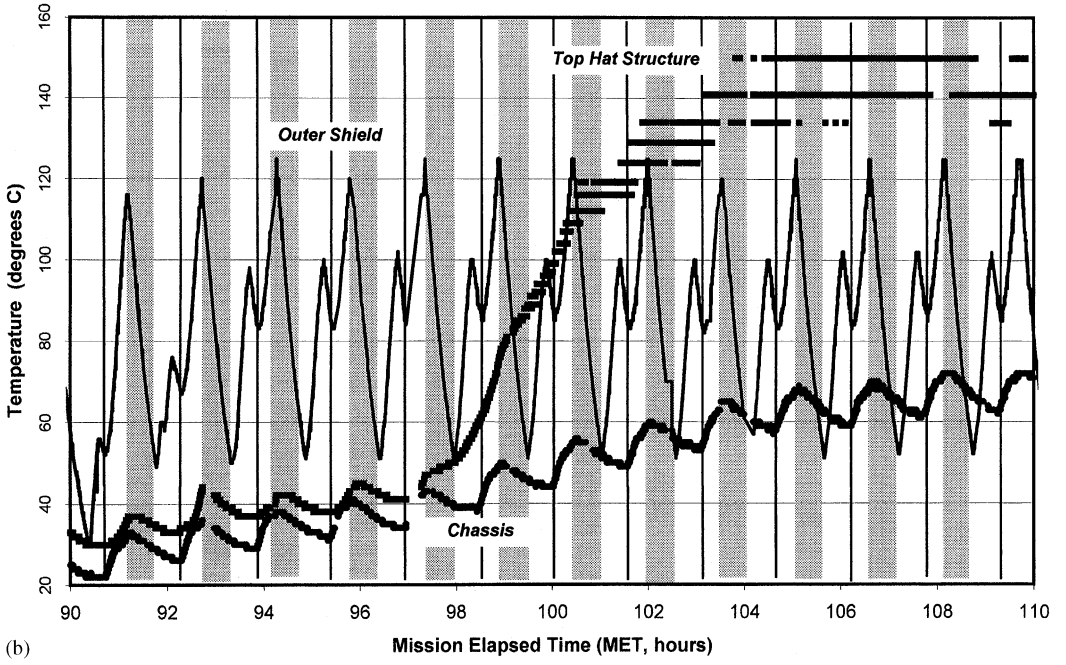

(b)

Fig. 10. (a) Expanded plots of wake side pressure for WSF-02 as measured by the Kernco gauge K2 (flux) and the inboard, B1, and outboard, B2, Balzers gauges for the time period 90–110 MET hours. Included are orbital sunrise and sunset as the edges of the darker sections denoting orbital night. In addition, orbital noon is denoted by the black lines. The onset of growth occurs at about 100 MET and is clearly manifest by the large changes in pressures recorded by the three gauges. (b) Expanded plots of wake side temperature for WSF-02 as measured by thermisters on the outer shield, chassis, and Top-hat for the time period 90–110 MET hours. Note the blip at noon for the outer shield and the increase in temperature of the Top-hat structure commencing with the initiation of the first growth phase for this flight.

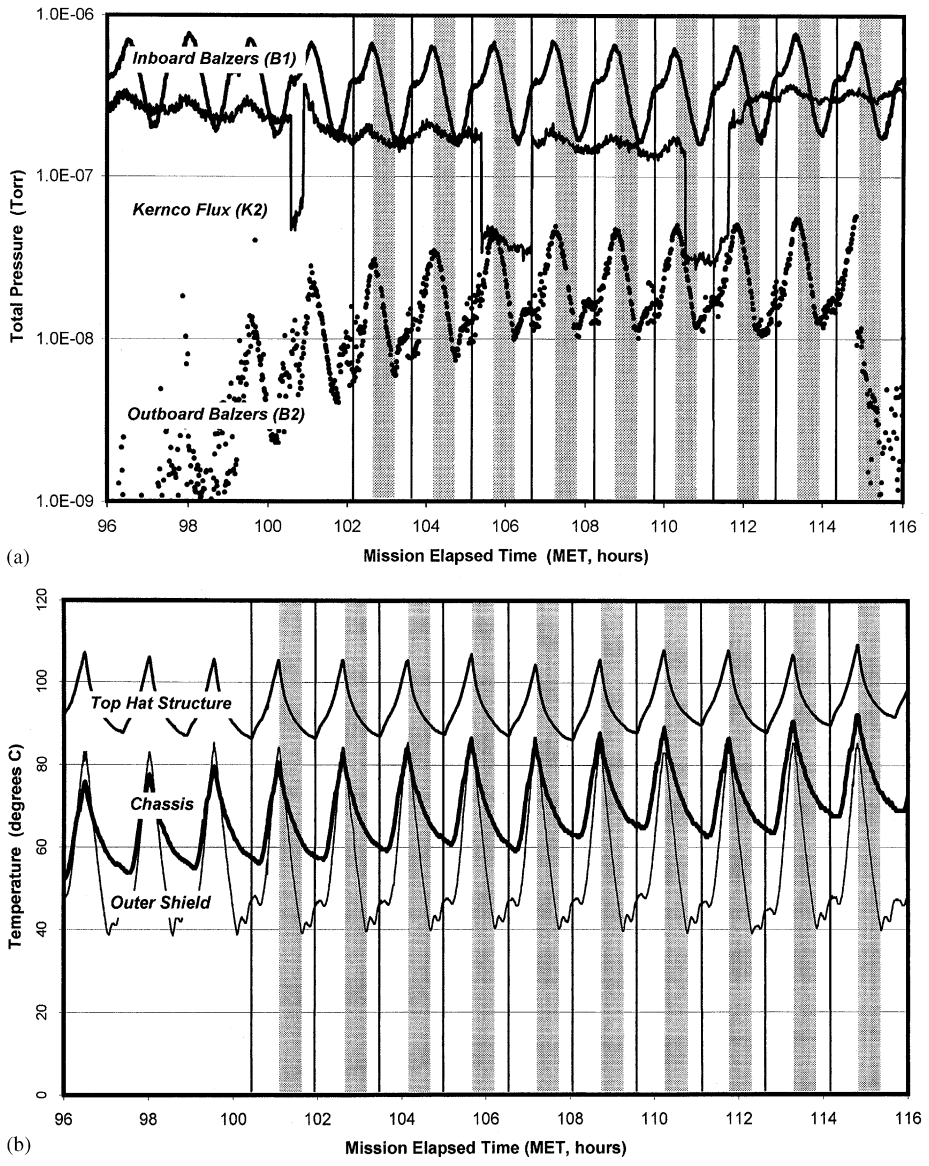

Fig. 11. (a) Expanded plots of wake side pressure for WSF-03 as measured by the Kernco gauge K2 (flux) and the inboard, B1, and outboard, B2, Balzers gauges for the time period 96–116 MET hours. Included are orbital sunrise and sunset as the edges of the darker sections denoting orbital night. In addition, orbital noon is denoted by the black lines. The onset of growth occurs at about 93 MET. Note that the pressures recorded by the Balzers gauges are an order of magnitude higher than in the WSF-02 flight, while the pressure recorded by the Kernco flux gauge is actually lower by about an order of magnitude. This is attributed to the gallium cell depletion during the beginning of the growth phase and the corresponding gallium coating of the chassis (see text). (b) Expanded plots of wake side temperature for WSF-03 as measured by thermisters on the outer shield, chassis, and Top-hat for the time period 96–116 MET hours. Note that the chassis diurnal variation is about twice that during WSF-02 and is attributed to the gallium coating (see text) caused by the run-away gallium cell. Also note that the Top-hat structure is fairly stable at lower temperatures than for WSF-02. This reflects the Top-hat redesign for WSF-03 to decrease the temperature increase during growth. Finally note that the blip at noon for the outer shield occurs at a lower relative temperature than for WSF-02. We speculate that this is due to the average sun angle in late November (WSF-03) being substantially less than in early September (WSF-02), so that shadowing of the shield near the thermister by other structures on the WSF could have occurred.

'bottomed out' (reached their lower measurable limit) at MET equal to 118 h. K2 began recording again during the second thin film growth sequence when the pressure became sufficiently high (MET 141–147 h).

The Balzers gauges tracked each other fairly well through the first thin film growth phase even though the maximum values of the inboard gauge B1 consistently read about a factor of ten higher than the maximum values of the outboard gauge B2.

After the first growth sequence, B2 continued to display the same diurnal variation and phase shift as the other gauges, but the shape of the pressure curves changed. Note that the average value of the pressure and the diurnal variation dropped below 1×10^{-9} Torr which is the lower practical pressure limit of the gauge. Thus even though the pressure data continued to exhibit a diurnal variation, its magnitude and shape are unreliable and we will not consider these data any further. It might be noted that the Balzers gauges electronics did not exhibit the decrease in gain with increase in WSF temperature that the Kernco gauges displayed [18].

3.3.2. WSF-03

On WSF-03, the initial pressure readings (Fig. 7a) were more or less the same as on WSF-02 (Fig. 6a). The inboard Balzers, B1, recorded 4×10^{-10} Torr and the outboard Balzers, B2, could not be determined as the pressure was well below its lower limit. The Kernco, K2, was also pegged at its lower limit. However, as the source cell assembly and the carousel warmed up (Fig. 7b—90 h MET), the base pressure measured by B1 monotonically rose to a value of 2×10^{-7} Torr (Fig. 7a—90 h MET), or about an order of magnitude higher than the WSF-02 base pressure during the same time period (warm-up, degas, and growth phases). Also, the base pressure measured by the outboard Balzers, B2, increased to about 1×10^{-8} Torr.

3.4. Summary

What could be the cause of both the high DC pressure values and any measurable diurnal pressure variation (especially of the order of $\Delta P/P \cong 100$) on the wake side? Recall that the wake vacuum concept should result in a decrease of the atmospheric constituents on the wake side by a factor of 10^4 for hydrogen and more than 10^8 for the heavier constituents (i.e. atomic oxygen, the main constituent). We considered five possibilities:

1. thermal desorption of adsorbed species from the wake side of the WSF by the sun which are then back-scattered from the source cell assembly structure into the pressure gauges;
2. photodesorption of adsorbed species from the wake side of the WSF by the sun;
3. back-scattering of the ambient atomic oxygen into the wake due to collisions at the wake edge with molecules outgassing and/or released from the WSF;
4. surface diffusion of absorbed species on the ram side around the edge onto the wake side; and
5. pressure gauges primarily measuring species which are outgassing from the walls of the gauge itself when heated, and not the flux of external particles into the gauge.

We will consider the last possibility first. The Balzers gauge used on the WSF is rated in its data sheet [15] as having a permissible ambient temperature when measuring, of 0–80°C. A rough calculation indicates that the variation of the temperature of the Balzers gauges themselves should be about 1/3 of the variation of the temperature of the shield to which they are attached. Thus the temperature excursion of the Balzers during flight should have been close to the data-sheet limits. Normally a cold-cathode gauge is used under conditions in which the temperature of the gauge is maintained more-or-less constant during pressure measurements. This was certainly not the case for those on board the WSF; moreover, the gauges were not outgassed prior to the measurements. Although cold-cathode gauges are known to pump and clean themselves up over time [19], it is entirely possible that internal outgassing due to heating, solar and otherwise, might have contributed significantly to the total pressure measured. In fact under conditions of high gauge temperature relative to external outgassing surfaces and/or high levels of contaminates

(water) in the gauges themselves, internal outgassing pressure might very well dominate any external pressure. Under these conditions the gauges would record essentially their internal outgassing pressure and not the external pressure.

Analysis of the temperature/pressure data gives conflicting evidence as to whether or not some fraction of the measured pressure was, in fact, internal outgassing. We give several examples. For the duration of both the flights, the DC value of the outer shield temperature remained constant (90°C for WSF-02 and 60°C for WSF-03). If the gauges, which are located on the outer shield, were reading only their own internal pressure, one would expect the base pressure (lowest value in the orbital cycle) and the DC values of the pressure to also remain constant. In fact both the base and DC values of the pressure changed significantly during the two flights. For WSF-02, the base value of B1 increased from release (at MET 90 h when it became a free flyer) from just below 1×10^{-9} Torr to 7×10^{-9} Torr just before the first growth (MET 100 h). During the first growth, the base pressure increased again to about 1×10^{-8} Torr reflecting the flux of As from the source cells. Obviously any internal outgassing in B1 was insufficient to mask a known minimum external increase in pressure of the order of 1×10^{-9} Torr. During the second growth run (MET 142–147 h) the base pressure rose abruptly from 1×10^{-9} to about 3×10^{-8} Torr, again reflecting the As flux from the source cells. More marked changes in the DC and base level were observed for WSF-03. For example, from release at MET 76 h to the start of the first growth at MET 92 h, the base pressure rose from 4×10^{-10} to 2×10^{-7} Torr. This could reflect either gas desorbing from internal surfaces of the gauges (internal outgassing) due to heating from sources other than the outer shield (note that B1 is very near the chassis) and/or from external surfaces (external outgassing) of the WSF due to heating during growth activity. In another example, pressure measurements in the ram position followed the pressure expected by the Jacchia model and not the temperature of the outer shield (Fig. 9). However, in this case external pressures on the ram side were expected to be quite high, so that internal outgassing, if present, might be insufficient to change the character of the measurements which reflected the external environment.

Finally it is easy to show that if there were *no internal outgassing*, the ratio of the pressures measured by the inner Balzers, B1, to the outer Balzers, B2 (which are at different radial positions on the shield) should remain relatively constant over an orbital period. This is true as long as there was no large external flux due to source cell activity. Moreover, this ratio can be easily calculated from the geometry of the WSF and is equal to about 4.6. On WSF-02 and WSF-03 the *experimental* pressure ratios varied with MET, on average, from 9.6 to 15.1 and 14.4 to 16.4, respectively. The lower number corresponds to the highest temperature and the higher number to the lowest temperature during an orbital period. This suggests that some fraction of the recorded pressure was due to internal outgassing. The data as recorded were insufficient to determine exactly the value of this fraction. However, an approximate analysis of the WSF-02 pressure data between MET 94 and 100 h indicates that the data are consistent with the possibility that from 10% to as high as 80% of the total recorded pressure could be due to internal outgassing, with the lower figure associated with the highest temperatures. One should note, however, that if the recorded pressure was almost *entirely* due to internal outgassing, the ratio could be almost any value depending on the relative amounts of internal outgassing between the two gauges. In that case the analysis based on ratios would not be appropriate. As we shall see, this is probably the situation on WSF-03 with the internal Balzers gauge and possibly the external Balzers gauge.

What we are suggesting here is that analysis of the pressure/temperature data alone cannot uniquely determine the fraction of experimentally measured pressure that is due to internal outgassing. The estimation of that fraction will have to await a calculation of the measured pressure, taking into account internal outgassing, and its comparison to the pressure data. This treatment will be presented in Section 5.3.

A rough estimate of the surface diffusion constant, D, of $5\times10^{-5}\,cm^2/s$ for CO on Ni(1 0 0) [20] at 300 K suggest that surface diffusion (possibility #4 above) is not responsible for the diurnal variation. Taking this value of D as representative of surface diffusion of any important species, one estimates that during one orbital period, the concentration peak due to surface diffusion would advance by about 0.5 cm towards the center of the wake side of the WSF. Thus any diurnal effect at a vacuum gauge due to diffusion creating a variation in concentration on the wake side of the WSF would be completely washed out as thermal desorption of species back-scattered into the gauges occurs from all surfaces of the wake side of the WSF.

Back-scattering of ambient oxygen (possibility #3) can be eliminated as a rough calculation estimate of the maximum flux of oxygen atoms which would back-scatter onto the wake side is of the order of 2×10^9 molecules/cm^2 s. This flux is equivalent to a partial pressure of 5×10^{-12} Torr. In this estimate, we assume that atomic oxygen is back-scattered by water molecules outgassing from the WSF.

Finally we can eliminate photodesorption (possibility #2), as the signature for photodesorption would be pressure readings which follow, in phase, the cosine of the sun angle with respect to the normal to the wake side of the WSF surface. In particular, as the WSF passes from orbital day to night, the pressure should drop abruptly to a constant value just after the sunset terminator and remain at that value until orbital noon when the pressure should begin to increase with the cosine of the sun angle. What is actually observed is that the maximum in the pressure peak occurs at or very close to the sunset terminator, and then slowly decays, reaching a minimum a little after orbital sunrise.

To conclude, we suggest that a combination of possibility #1, thermal desorption of adsorbed species from the WSF, and possibility #5, thermal desorption of adsorbed species internal to the pressure gauges is the mechanism for the high DC and diurnal pressure variations measured by the pressure gauges.

4. Thermal desorption model

To explain both the diurnal variation and the slow variation (DC) in the *external component* of the measured pressure, we propose a thermal desorption model. We include both desorption from primary surfaces (those looking directly at the pressure gauges) and from secondary surfaces via single scattering (reflection and/or adsorption/readmission) from the primary surfaces. The sources of heat are the sun, which gives rise to the diurnal pressure variation, and the MBE assembly, which gives rise to the slow varying component of the pressure.

4.1. Pressure term

Diurnal solar heating outgasses the wake side and a fraction of the outgassed species are scattered from those parts of the WSF which are in direct line of sight of the pressure gauges. In particular, the equivalent pressure, P_j (in Torr) measured at the jth location due to a flux of species which are first outgassed from surfaces on the wake side of the WSF and then back-scattered into the pressure gauges is given by

$$P_j = k\sum_i g_{j,i}\phi_i, \tag{1}$$

where $g_{j,i}$ is a geometric constant relating the ith outgassing surface to the jth pressure location, ϕ_i is the outgassing or desorption rate in molecules/cm^2 s from the ith surface, and k is a conversion constant from flux to pressure equal to 2.6×10^{-21} Torr cm^2 s/molecules at 300 K. This equation can be derived and the geometric constants $g_{j,i}$ determined from the fundamental relation giving the flow of particles from a small area dA_i to a second small area dA_j under the conditions of molecular flow [21]:

$$\Psi_j = \phi_i\cos\beta_i\cos\beta_j\,dA_i\,dA_j/(\pi r^2). \tag{1b}$$

Here Ψ_j is the flux incident on dA_j, ϕ_i is the flux leaving surface dA_i, r is the distance vector between the two small surfaces, and β_i and β_j are the angles between the normals to dA_i and dA_j, and the vector r.

From Eq. (1b), it can be seen that up to single scattering, the geometric factor $g_{j,i}$ can be approximated as the sum of products of two terms

$$g_{j,i} \cong \sum_k S_P(r_k, r_i) S_S(r_j, r_k), \tag{1c}$$

which depend on the geometry of the surfaces in question (in this case the outer surfaces of the WSF) and the position, j, on the object where the pressure is to be inferred or measured. In particular the first term, $S_P(r_k, r_i)$, is the integral of the solid angle subtended by all primary outgassing surfaces denoted by r_i measured from any secondary outgassing surface at r_k, which is in direct line of sight of the pressure gauge and the second factor, $S_S(r_j, r_k)$, is the solid angle subtended by the pressure gauge at position j, from a secondary outgassing surface at r_k in direct line of sight of the pressure gauge (or wherever the pressure is to be calculated).

The principal primary outgassing surfaces on the wake side of the WSF are the MBE growth assembly and the shield itself. The principal secondary scattering surfaces on the wake side of the WSF are those associated with the MBE growth assembly. In first-order processes, molecules desorb from the MBE growth assembly and directly impinge on the pressure gauges if these surfaces are in direct line of sight. In second-order processes, molecules desorb from the wake shield itself and are scattered back onto the pressure gauges by the MBE growth assembly.

For the purpose of calculating the geometric factors, the MBE growth assembly is broken down into three components: the Top-hat assembly, the source-cell assembly, and the MBE support structure (Fig. 3). The Top-hat assembly is modeled as a cylinder of height 0.95 ft and diameter 1.2 ft. The source-cell assembly is modeled as a truncated cone of height 0.88 ft, and top and bottom diameters 1.2 and 0.44 ft, respectively. At full power the outside of the source-cell assembly reaches a temperature of about 600°C. The MBE support structure is modeled as eight rods, the struts, of cross-section width 1 in and length 2.53 ft. Its temperature as a function of time was not measured but assumed here to be similar to that of the outer shield. The temperature dependencies of the Top-hat, chassis, and shield for flights WSF-02 and WSF-03 are given in Figs. 6b and 7b. The Top-hat sits on top of the source-cell assembly. The distance from the center of the substrate (center of the WSF) to the center of the bottom of the source-cell assembly is taken as 0.67 ft. Finally the diameter of the WSF is taken as 12 ft and the distances from the center to Balzers gauges B1 and B2 are taken to be 2.93 and 5.92 ft, respectively.

Under equilibrium conditions (as many secondary scattered molecules leave a secondary outgassing surface as are incident on that surface), a computer calculation (with certain approximations) yields the values of $S_{j,i}$ given in Table 1.

Each of the terms above represents an integral over the surfaces noted. The notation $S_{j,i}$ indicates scattering from the ith surface to the jth surface. For example, to calculate the pressure at the location of the inside Balzers gauge, B1, one would put together the following terms:

$$\begin{aligned} P_{B1} = k[&S_{B1,TH} S_{TH,S} \phi_S + S_{B1,TH} \phi_{TH} \\ &+ S_{B1,SCS} S_{SCS,S} \phi_S + S_{B1,SCS} \phi_{SCS} \\ &+ S_{B1,SCB} S_{SCB,S} \phi_S + S_{B1,SCB} \phi_{SCB}], \end{aligned}$$

where the subscripts refer to the primary and secondary outgassing surfaces, i.e. S = shield, TH = Top-hat, SCS = source-cell side, etc.

4.2. Temperature term—outgassing rates

In order to complete the calculation, we must estimate the outgassing or desorption rate, ϕ_i, of the ith surface which is highly dependent on both temperature and history. We can separate out the temperature dependence from the history factors by writing (see for example [22])

$$\phi_i = Q_i \exp(-E_{des}/kT_i)/(\exp(-E_{des}/kT_c). \tag{2}$$

Here Q_i is the desorption rate of the ith surface at constant temperature T_c, E_{des} the desorption activation energy, and T_i the temperature.

A review of the literature suggests that outgassing rates at room temperature for water and other species adsorbed on stainless steel can vary over more than seven orders of magnitude (3.9×10^{13}–8×10^5 molecules/cm^2 s) [3,19,23–25], depending on such history factors as the details of

Table 1
Values of the important solid angle integrals $S_{j,i}$ as noted in Eq. (1c) in the text. Each term represents an integral over the surfaces noted. The notation $S_{j,i}$ indicates scattering from the ith surface to the jth surface

$i \Downarrow j \Rightarrow$	Top-hat	Source C, side	Source C, bottom	Struts	Chassis	Shield	Carousel	Balzers in	Balzers out
Top-hat	1.0	0.0	0.0	0.0	0.0063	0.0083	0.0	0.0166	0.0041
Source C, side	0.0	1.0	0.0	0.0	0.0691	0.0034	0.0	0.0069	0.0011
Source C, bottom	0.0	0.0	1.0	0.0	0.0036	0.0001	0.0977	0.00028	0.00002
Struts	0.0	0.0	0.0	1.0	0.0	0.0	0.0538	0.0	0.0
Chassis	0.1007	0.328	0.947	0.0	1.0	0.0	0.0	0.0	0.0
Shield	0.166	0.168	0.041	0.0	0.0	1.0	0.0	0.0	0.0
Carousel	0.0	0.0	0.303	0.0	0.0	0.0	1.0	0.0	0.0
Balzers in	0.0	0.0	0.0	0.0	0.0	0.0	0.0	0.0	0.0
Balzers out	0.0	0.0	0.0	0.0	0.0	0.0	0.0	0.0	0.0

the surface treatment, prior exposure to water vapor, and the pumping time and degree of baking prior to measurement. The primary mechanism responsible for the outgassing appears to be water diffusing through the passivation oxide layer to the surface [26,27].

An additional complication arises in the relationship of the *true* outgassing rate to the *measured* outgassing rate [28,29]. Most measurements of outgassing rates are done by either the throughput or the pressure rise method. In these cases the measured outgassing rate is the difference between the true outgassing rate and the readsorption rate [28]. Hobson [28], Redhead [29,30], and others have shown that the true outgassing rate can be from one to three orders of magnitude larger than the net or measured rate [28–30]. In addition, Komiya et al. [31] have directly measured the true outgassing rate from unbaked 304L stainless steel at room temperature using a molecular beam system with cryogenic baffles in which readsorption was not allowed to occur. They found outgassing rates 10–10^2 larger than values previously reported, in accordance with Hobson and Redhead. In the following section, we will present outgassing rates from 304L stainless steel using both techniques.

A comprehensive literature survey of outgassing from stainless steel was done by Dylla et al. [23,26,27] in 1993. By fitting a large amount (some 22 results) of experimental data, they deduced an empirical expression for the outgassing rate, Q, as a function of pumping time from 304L stainless steel. All samples had first been cleaned, baked, cooled, and vented to 1 atm of air for 1 h before being pumped down. No correction was made between the measured rates and the reported rates. Their result for outgassing rate is

$$Q = Q_0 t^{-n}, \tag{3}$$

where time, t, is given in minutes and the exponent, n, is approximately equal to 1 for unbaked systems. The best value they found for the constant Q_0 is 6×10^{12} molecules/cm^2 s. They also determined that the outgassing was dominated ($>85\%$) by water (H_2O). Their expression yields the values tabulated in Table 2. The measurements of the true outgassing rates as reported by Komiya et al. [31] are also included.

Note that Komiya et al.'s values are about two and a half orders of magnitude larger than those reported by Dyalla et al., in agreement with the theoretical work of Hobson, Redhead, and others.

For completeness, we list other values for outgassing rates of 304L stainless steel as found in the literature in Table 3.

Although each original reference was not checked in detail, we will assume that the values above refer to *net* or *measured* outgassing rates and not the true rates.

Obviously the measured outgassing rates of water from 304L stainless steel span an enormous range, depending on the particular history of the sample and the technique used to make the measurement.

Table 2
Values of the outgassing rate, Q, as a function of pumping time from 304L stainless steel at room temperature

Time	Q (molecules/cm^2 s) (Dylla et al. [23])	Q (Komiya et al. [31])
1 min	6.0×10^{12}	—
1 h	1.0×10^{11}	3.9×10^{13}
10 h	1.0×10^{10}	5.0×10^{12}
24 h	4.2×10^{9}	2.4×10^{12}
75 h	1.3×10^{9}	8.7×10^{11}
100 h	1.0×10^{9}	6.3×10^{11}
1000 h	1.0×10^{8}	—

Table 3
Representative values of outgassing rates for 304L stainless steel as found in the literature

Time/treatment	Q (molecules/cm^2 s)
1 h pump	7.9×10^{12} [24]
1 h pump	5.25×10^{11} [19]
5 h pump	10.5×10^{10} [19]
10 h pump	5.25×10^{10} [19]
75 h pump	1.55×10^{9} [25]
Thoroughly degassed	3.0×10^{7} [3]
Degassed at 400°C–20 h	0.81×10^{6} [25]

5. Data analysis

We are now in a position to calculate the pressure at any point on the WSF provided we know the outgassing rates and temperature of each surface which can contribute to the gas load. Since we have data for the temperature of most of the surfaces on the WSF as a function of time for the entire flight (Figs. 6b, 7b, 10b and 11b), we can use the model to calculate the first-order pressure at any point on the WSF for any time. We first assume that the outgassing rates at room temperature are as given in the previous section. We then use the model to calculate both the DC values of the pressure at any point, as well as the expected diurnal variation.

5.1. Desorption energy estimate

If indeed the diurnal pressure variation is due to thermal outgassing by the sun, the diurnal pressure variation data should give us information about the desorption energy of the major outgassing species. Combining Eqs. (1) and (2) we obtain

$$P_j(T) = kG_{j,total}Q\exp(-E_{des}/kT)/(\exp(-E_{des}/kT_c), \tag{4}$$

where we have assumed that the temperature, T, and the outgassing rate are the same for *all* primary surfaces and

$$G_{j,total} = \sum_i g_{j,i}$$

is the sum over all surfaces which are in direct line of sight of the pressure gauge and the location j. If we now calculate the fractional change in pressure, $\Delta P/P$, over an orbital period, we get

$$\ln(1 + \Delta P/P) = (E_{des}/kT_H)(\Delta T/T_L) \tag{5}$$

which is independent of both the outgassing rate and the geometric constant ($kG_{j,total}Q$) provided that the outgassing rate is the *same* for all primary surfaces. In this expression, T_L and T_H are the low and high temperatures respectively.

In comparing to WSF data, we must select pressure data where the temperatures of the primary outgassing surfaces are more or less the same. This condition would suggest times when there were no MBE thin film growth operations. We thus chose a time at the beginning of the free flight of WSF-02 and at the end of WSF-03 when there is no growth and the source cell assembly and the carousel are not being heated. A look at the pressure data in Fig. 10a between 90 and 94 h indicates that over one orbital period, $\Delta P/P \cong 100$. The temperature data in Fig. 10b yield the values for T_L and T_H to be 50°C and 120°C. Substituting both of these data in Eq. (5) we find that E_{des} is about 0.84 ev (19.4 kcal/mol), a value which lies within the range of desorption energies of water as reported in the literature [32] (19–23 kcal/mol). This strongly supports the conjecture that the cause of the wake side diurnal pressure variation is thermal outgassing of water by the sun. Applying the analysis to flight WSF-03 data between 146 and 150 hours yields a somewhat smaller value of E_{des} (0.72 eV). Note that in this case a large fraction of the measured pressure is most likely due to internal and not external outgassing.

However this should not affect the analysis as long as the majority of outgassing species is the same internal to the gauge as external from the WSF surfaces.

5.2. Base pressure analysis

We can also use Eq. (4) to estimate the base pressure on the wake side due to outgassing from the WSF itself before any heating by the MBE equipment has begun. If we assume that all outgassing surfaces are at the same temperature and they have the same outgassing rate, we can sum over the geometrical constants, $g_{j,i}$, creating a total geometrical constant, $G_{j,total}$, for each location, j, at which the pressure is to be estimated. In addition, we take the outgassing rates as given by Komiya et al. [31] for 1, 10, and 100 h pumping on unbaked 304L stainless steel at room temperature (21°C). The values of the estimated pressures at these times together with the calculated value for the summed geometrical constant are given in Table 4.

The comparisons with the experimental data from WSF-02 ($B1 = 2 \times 10^{-9}$ Torr and $B2 = 4 \times 10^{-10}$ Torr) and WSF-03 ($B1 = 4 \times 10^{-10}$ Torr, B2 out of range) are bracketed by equivalent pumping times of about 1–10 h. In fact the amount of time between unberth (initial exposure of the WSF to the vacuum in orbit) and when the initial pressure measurements were made was about 10 h for WSF-02 and about 2 h for WSF-03. Thus, the above predicted pressure values compare well with the experimental values, and lend support to the credibility of the proposed thermal model incorporating WSF outgassing.

It is well to note that a calculation using the model with variable outgassing rates suggests that the ultimate low pressure possible on the wake side of the WSF is limited only by outgassing from the WSF itself. Notwithstanding the higher than expected pressures recorded on WSF-02 and WSF-03 and confirmed by the thermal model, this ultimate pressure could approach 1×10^{-14} Torr if means, such as longer time on orbit, were found to reduce the outgassing of water and other species to the lower limits found in the literature (i.e., less than 3×10^7 molecules/cm^2 s as in Refs. [3,24] in the above table).

5.3. Diurnal pressure analysis

Finally, we have used the thermal desorption model (Eq. (1)) to calculate the pressure at the Balzers gauges as a function of time using the time-dependent temperature data gathered during the flights. In order to make a reasonable fit with the data, especially for WSF-03, it was necessary to include internal outgassing in the pressure gauges.

5.3.1. Internal gauge outgassing

We were led to consider internal outgassing from the large increase in recorded pressure with source cell and sample heating that could not be reasonably modeled using the thermal desorption model described in Section 4. In particular, WSF-03 Balzers total pressure gauges report an order of magnitude greater pressure than those reported on WSF-02. The DC component of WSF-03 inboard Balzers pressure readings rose in close correlation with elevated chassis temperatures (relative to WSF-02), suggesting gauge behavior that is highly

Table 4
Values of calculated base pressures at selected locations and times on the wake side of the WSF together with the calculated values for the summed geometric constants (see text)

	Balzers #2 out		
	Substrate	Balzers #1 in	Balzers #2 out
$G_{j,total}$	0.263	0.0314	0.00686
P (1 h)	2.6×10^{-8} Torr	3.18×10^{-9} Torr	6.96×10^{-10} Torr
P (10 h)	3.42×10^{-9} Torr	4.08×10^{-10} Torr	8.92×10^{-11} Torr
P (100 h)	4.31×10^{-10} Torr	5.14×10^{-11} Torr	1.12×10^{-11} Torr

temperature dependent, and post-flight testing was performed to quantify the relationship [18].

Using a test configuration designed to mimic both the magnitude and dynamics of on orbit temperature excursions, the Balzers gauges were mounted (without outgassing) on a cryopumped chamber used for device calibration throughout the Wake Shield Program, and monitored with a mass spectrometer and nude ion pressure gauge. Chamber background pressures were held at 2×10^{-9} during several independent trial runs to simulate the WSF low earth orbit wake side environment, while a controllable heat source varied the temperature of the Balzers gauge mounting flange. Results of a typical test run are given in Fig. 12 and show a significant increase in *measured* pressure as a function of increased gauge temperature. Finite thermal conduction between the mounting flange and the internal surface surrounding the gauge's ionization volume is evidenced by the hysteresis of a *P versus 1/T* plot of the same data in Fig. 13.

The temperature tests on the Balzers gauges are consistent with the variations in in-flight pressure readings during WSF-03, given the reasonable assumption that the Balzers inboard gauge temperatures are comparable to that of the chassis temperature (maximum average value of 75°C) on WSF-03. Fig. 14 displays inboard gauge flight pressure data during the mission when chassis temperatures were in the 75°C range. The large variation of pressure with time is consistent with heating of the Balzers gauge as a result of diurnal heating of the chassis and resultant increase of *measured* pressure similar to that seen in the lab tests of Fig. 12.

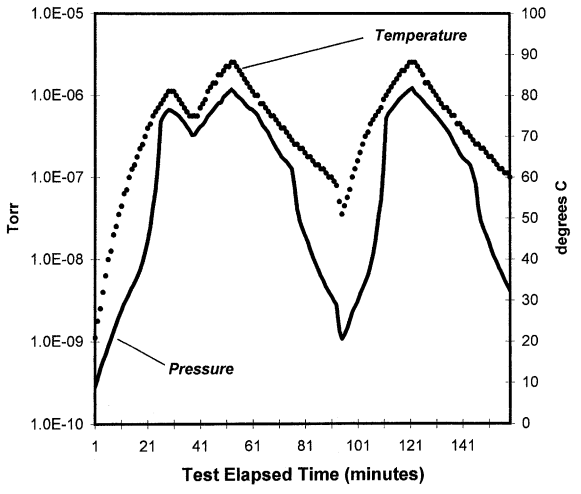

Fig. 12. Typical post-flight test pressure readings of the Balzers gauge as a function of temperature. The temperature was varied to simulate the actual temperature variation during an orbital period.

5.3.2. Calculation parameters

The external pressures at WSF were calculated from Eq. (1) with the values of ϕ_I calculated from Eq. (2). The temperatures of the appropriate surfaces as a function of time are taken from the flight temperature data. The outgassing rate at constant temperature is given by Eq. (3), and we chose the value of Q_0 as measured by Komiya et al. since his experiment measured the *true* outgassing rate from unbaked stainless steel. The start of the outgassing time was taken as the launch time, as that is when the WSF was shortly (within $\sim$8 min) exposed to a vacuum of about 1×10^{-5} Torr in the

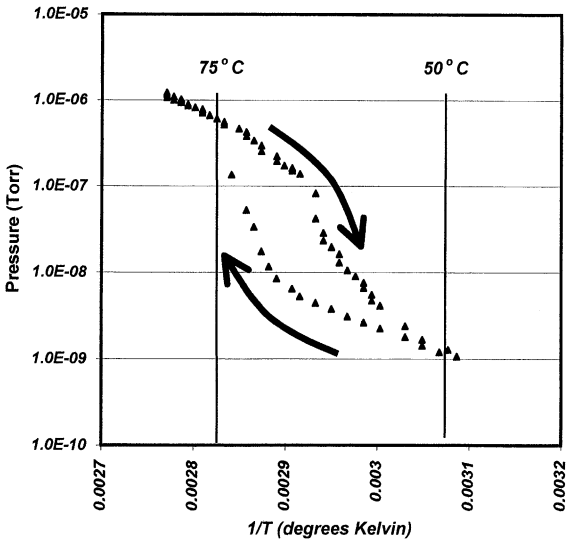

Fig. 13. Post-flight test plot of Balzers gauge pressure versus the reciprocal temperature. Note the hysteresis due to finite thermal conduction between mounting flange and the internal surface surrounding the gauge's ionization volume. These plots were used to calculate the increased pressure measured by the Balzers gauges due to internal outgassing.

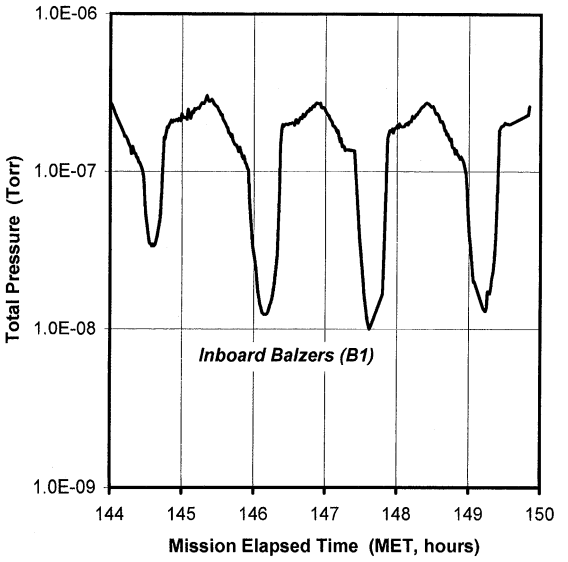

Fig. 14. Inboard Balzers gauge data recorded during WSF-03 when the chassis temperature was in the 75°C range (MET between 144 and 150 h). The large variation of pressure with time is consistent with the test run shown in Fig. 12 and lends support to the possibility that for WSF-03 a substantial fraction of the recorded pressure by the Balzers gauges was due to internal outgassing.

cargo bay. Finally, we considered as the primary surfaces, the shield and chassis, and as the secondary surfaces, the Top-hat assembly and carousel. In this choice we assumed that the secondary surfaces were sufficiently outgassed when the sample and source cells were brought up to temperature prior to actual growth.

The inclusion of internal outgassing in the gauges themselves was done by modeling the experimental heating results of the Balzers gauge plotted in Fig. 13, and adding the resulting *measured* pressure to the calculated external pressure. The dc gauge temperature for the internal Balzers (B1) was taken as equal to the average of the dc shield and chassis temperature, and included 1/3 of the ac average of the outer shield and chassis temperature. The justification was that the internal Balzers was mounted on the shield next to the chassis. To affect a reasonable fit to the data, the external Balzers (B2) required a much smaller fraction of internal outgassing. Indeed this gauge produced a fair amount of erratic data, so that any conclusions from analysis of its data are probably unreliable.

5.3.3. Comparison with experiment

Using the time-dependent flight temperature data for WSF-02, the *calculated* values of both external pressure (the pressure calculated from the thermal desorption model) and total pressure (with the inclusion of internal outgassing) at the position of the inboard Balzers gauge (B1) are plotted in Fig. 15 as a function of time (MET) for the entire flight. Comparison of the *calculated* pressures with the *flight data* pressures for WSF-02 and WSF-03 is presented in Fig. 16a and b for the entire flights. Reasonable agreement is seen between these calculated *total* pressure curves and the experimental data in terms of the phase, magnitude, and overall shape of the diurnal pressure variation. Passable agreement is seen in the overall shape of the complete mission pressure curves with respect to the heating and cooling of the MBE apparatus.

In particular, solar thermal desorption, both external and internal, can indeed explain the phase shift in the wake side pressure data relative to the ram side data. It should be noted that the pressure peak on the wake side occurs at, or very close to, the sunset terminator (see Fig. 10a) or about 27.9 min after solar noon (with respect to the WSF in orbit) which is about 1/3 of an orbit. On the other hand, the ram side pressure peak occurs at about 2:00 p.m. local time in complete accord with the Jacchia 1970 model for atmospheric density due to solar heating.

The improvement in agreement between the calculations and the flight pressure data, after adding the internal outgassing contribution, suggests that, at least for WSF-03, the pressure gauges were not sufficiently outgassed prior to launch. Also it seems reasonable to attribute the increased diurnal variation in the chassis temperature to gallium coating the surface. Indeed the measured pressure values for WSF-03 probably consisted of better than 95% of its readings due to internal outgassing. On the other hand, the gauges appear to have been much cleaner and somewhat cooler during flight WSF-02 so that the measured

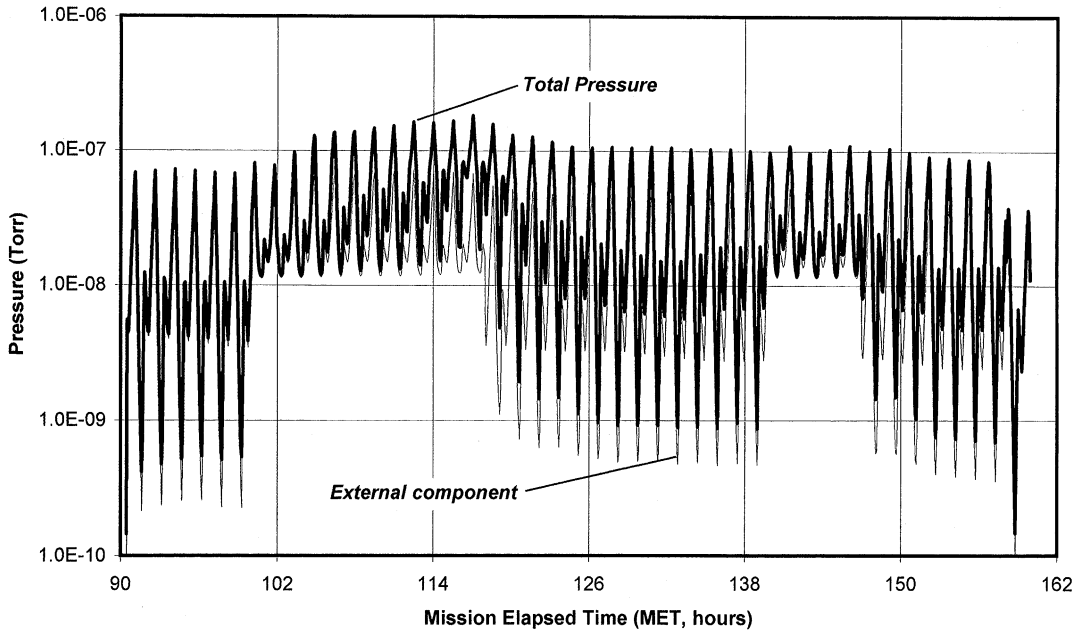

Fig. 15. Calculation of both external pressure and total (external plus internal gauge outgassing) pressure for the Balzers inboard gauge, B2, plotted as a function of MET for the entire WSF-02 flight. Note that at higher pressures, up to 50% of the total pressure is due to internal gauge outgassing. Typical pressure values are somewhat less than that, averaging about 20–30% internal gauge outgassing.

pressure averaged about 50% of its values due to internal outgassing.

6. Conclusions

There are two important conclusions to be drawn from this work. First, the results of the ram side pressure data appear to be the first direct verification of the Jacchia atmospheric density model used over the years for calculating satellite drag and other orbital parameters. For the first time atmospheric density at about 250 miles altitude was measured directly during many day/night cycles as the WSF orbited about the earth.

Second, the pressure results on the wake side validate the wake vacuum concept, as the pressure on the wake side is greatly reduced over the pressure on the ram side. The ram side and wake side variations are both caused by the heating of the sun, but the ram side variation is due to the WSF moving through a time-varying atmospheric density (due to the sun heating the atmosphere), while the wake side variation is due to the sun thermally outgassing water from the wake side stainless steel shield and other components including the gauges themselves. The only cross-talk occurs when the outgassing water molecules collide with the species in the ambient atmosphere (mostly atomic oxygen) causing a small fraction to backscatter into the wake side. This process is proportional to the product of the density of the ambient atmosphere and the density of the outgassing water molecules, and becomes negligible in the limit that the density of outgassing water molecules becomes small. Therefore, if the wake side of the WSF is sufficiently outgassed (primarily of water), e.g. by baking and/or by an extended time on-orbit so that the outgassing rate is less than 3×10^7 molecules/cm^2 s, then total pressures of 1×10^{-14} Torr on the wake side of the WSF are certainly possible.

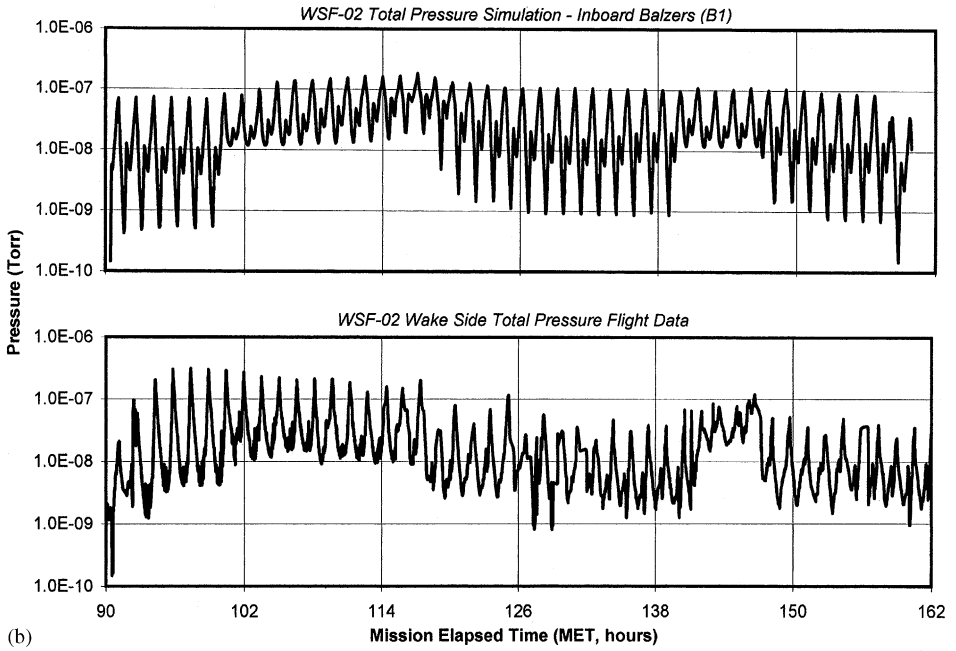

(b)

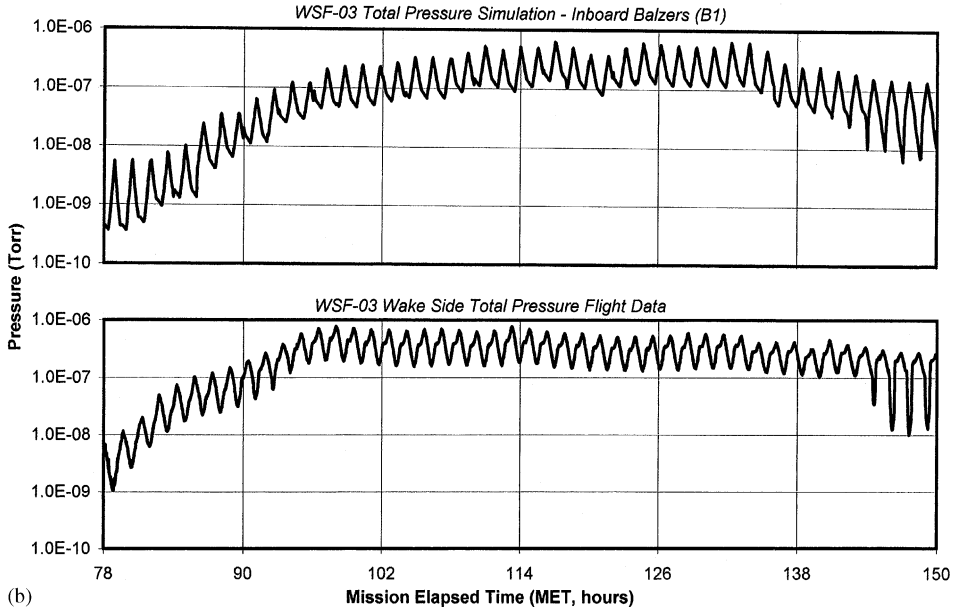

(b)

Fig. 16. (a) Comparison of the total calculated pressure (external plus internal gauge outgassing) with the flight pressure data from the inboard Balzers B1 for the entire flight of WSF-02. The agreement is within a factor of 2 or 3. (b) Comparison of the total calculated pressure (external plus internal gauge outgassing) with the flight pressure data from inboard Balzers B1 for the entire flight of WSF-03. Again the agreement is reasonable except that this comparison suggests that up to 90–95% of the flight recorded pressure is probably due to internal gauge outgassing. The difference between WSF-02 and WSF-03 was that the chassis and other surfaces in direct line of sight of the gallium source cell became coated with gallium early in the flight and subsequently got hotter than in WSF-02. The higher temperatures of the Balzer gauge, especially the outer excursions of the diurnal variation, resulted in much higher levels of internal outgassing which was recorded as increased measured pressure.

Acknowledgements

The authors would like to acknowledge Jorge Aguilar, Ralph Cox, Charles Horton, Art Rabeau and the WSF project engineering team at Space Industries, Inc. for their contributions to the flight experiment. Strong support for this program by personnel at NASA Johnson Space Center is greatly acknowledged with specific thanks to the flight operations community and the flight crews that have been involved in making the WSF fly. Funding support from NASA, from the SVEC industry consortium members involved in the WSF program, and from the State of Texas is very greatly acknowledged.

References

[1] Wuencher HF. New Sci 1970;47:54.
[2] Melfi LT, Outlaw RA, Hueser JE, Brock FJ. J Vac Sci Technol 1976; 13:698.
[3] Hueser JE, Brock FJ. J Vac Sci Technol 1976;13:702.
[4] Naumann RJ. J Vac Sci Technol 1989;A7:90.
[5] Ignatiev A, Chu CW. Metall Trans 1988;19A:2639.
[6] Ignatiev A. Adv Mater Manuf Process 1988;3:599.
[7] Ignatiev A. Space commerce '92. Montreaux: Gordon and Breach, 1992.
[8] Ignatiev A. Earth Space Rev 1995;4:10.
[9] Cho AY, Arthur JR. Prog Solid State Chem 1975;10:157.
[10] Justiz CR. PhD thesis, Department of Physics, University of Houston, 1993.
[11] Justiz CR, Sega RM, Dalton C, Ignatiev A. Proceedings of the AIAA 27th Thermophys Conference AIAA 92-2935, 1992. p. 2935.
[12] Jacchia LG. Smithson. Astrophys. Obs. Spec. Rept. No. 332, 1971.
[13] Jacchia LG. Smithson. Astrophys. Obs. Spec. Rept. No. 375, 1977.
[14] Kernco Catalog, CCIG S/N 003.
[15] Balzers Catalog, IKR 020 cold cathode gauge heads, part # DN 35 CF-F, Balzers AG, Liechtenstein.
[16] Horton C, Aguilar J, Cox R. Total pressure gauge calibration report, SVEC, 1995.
[17] Cox R. SVEC, University of Houston, unpublished data, 1996.
[18] Sterling M, Horton C. SVEC, University of Houston, unpublished data, 1998.
[19] Berman A. Total pressure measurements in vacuum technology. Orlando: Academic Press, Inc., 1985. p. 216.
[20] Zhdanov VP. Elementary physicochemical processes on solid surfaces. New York: Plenum Press, 1991. p. 52.
[21] Holkeboer DH, Jones DW, Fagano F, Santeler DJ. Vaccum technology and space simulation. New York: American Institute of Physics, 1993. p. 28.
[22] Somorjai GA. Chemistry in two dimensions: surfaces. Ithaca, NY: Cornell University Press, 1981. p. 78.
[23] Dylla HF, Manus DM, LaMarche PM. J Vac Sci Technol 1993;A11:2623.
[24] Vacuum Manual, TJ940.H63, 1974.
[25] Nuvolone R. J Vac Sci Technol 1977;14:210.
[26] Li M, Dylla HF. J Vac Sci Technol 1993;A11:1702.
[27] Li M, Dylla HF. J Vac Sci Technol 1994;A12:1772.
[28] Hobson JP. J Vac Sci Technol 1979;16:84.
[29] Redhead PA. J Vac Sci Technol 1996;A14:2599.
[30] Redhead PA. J Vac Sci Technol 1994;A13:467.
[31] Komiya S, Ugiyama Y, Kobayashi M, Tuzi Y. J Vac Sci Technol 1979;16:689.
[32] Chun I, Cho B, Chung S. J Vac Sci Technol 1996;A14:2636.